Biology of Human Tumors

Clinical Cancer Research

Combined Tumor Suppressor Defects Characterize Clinically Defined Aggressive Variant Prostate Cancers

Ana M. Aparicio[1], Li Shen[2], Elsa Li Ning Tapia[1], Jing-Fang Lu[1], Hsiang-Chun Chen[3], Jiexin Zhang[2], Guanglin Wu[1], Xuemei Wang[3], Patricia Troncoso[4], Paul Corn[1], Timothy C. Thompson[1], Bradley Broom[2], Keith Baggerly[2,5], Sankar N. Maity[1,6], and Christopher J. Logothetis[1]

Abstract

Purpose: Morphologically heterogeneous prostate cancers that behave clinically like small-cell prostate cancers (SCPC) share their chemotherapy responsiveness. We asked whether these clinically defined, morphologically diverse, "aggressive variant prostate cancer (AVPC)" also share molecular features with SCPC.

Experimental Design: Fifty-nine prostate cancer samples from 40 clinical trial participants meeting AVPC criteria, and 8 patient-tumor derived xenografts (PDX) from 6 of them, were stained for markers aberrantly expressed in SCPC. DNA from 36 and 8 PDX was analyzed by Oncoscan for copy number gains (CNG) and losses (CNL). We used the AVPC PDX to expand observations and referenced publicly available datasets to arrive at a candidate molecular signature for the AVPC.

Results: Irrespective of morphology, Ki67 and Tp53 stained $\geq$10% cells in 80% and 41% of samples, respectively. RB1 stained <10% cells in 61% of samples and AR in 36%. *MYC* (surrogate for 8q) CNG and *RB1* CNL showed in 54% of 44 samples each and *PTEN* CNL in 48%. All but 1 of 8 PDX bore Tp53 missense mutations. *RB1* CNL was the strongest discriminator between unselected castration-resistant prostate cancer (CRPC) and the AVPC. Combined alterations in *RB1*, *Tp53*, and/or *PTEN* were more frequent in the AVPC than in unselected CRPC and in The Cancer Genome Atlas samples.

Conclusions: Clinically defined AVPC share molecular features with SCPC and are characterized by combined alterations in *RB1*, *Tp53*, and/or *PTEN*. *Clin Cancer Res; 22(6); 1520–30. ©2015 AACR.*

Introduction

Understanding the therapeutically relevant biologic heterogeneity of common adult solid tumors led to the successful introduction of molecularly targeted agents. This is most notable in breast cancer (ER and HER2 overexpression; refs. 1, 2) lung cancer (EGFR mutations and EML4-ALK translocations; refs. 3, 4), melanoma (BRAF mutations; ref. 5), and colon cancers (RAS mutations; ref. 6). In prostate cancer, however, the prevalent "prognostic model" based on clinical features continues to frame clinical decision making (7). This can be attributed in part to the perception that the majority of men with prostate cancer uniformly benefit from androgen ablation and, perhaps more so, to the limited access to metastatic tissue needed for clinical, pathologic, and molecular correlations. However, the diverse responses to recently approved therapies with distinct mechanisms of action (e.g., second-generation androgen biosynthesis inhibitors) has exposed the biologic heterogeneity of prostate cancer and illustrates the urgent need to apply our understanding of prostate carcinogenesis to clinical decision making.

To overcome the challenge of tissue acquisition in metastatic prostate cancer and gain insight into the various clinical phenotypes observed, we initiated a comprehensive approach for tissue collection, clinical annotation, and development of patient tumor–derived xenografts (PDX). Here we describe the molecular characterization of a subset of prostate cancer with aggressive clinical behavior. Virulent prostate cancers with atypical (variant) clinical features have long been associated with small-cell prostate carcinoma (SCPC) morphology (8). More recently, we extended these observations in a prospective study (NCT00514540) that showed that aggressive prostate cancers of various morphologies sharing clinical features with the SCPCs (termed anaplastic prostate carcinomas or aggressive variant prostate carcinomas, AVPCs) also displayed a high responsiveness to chemotherapy (9). The shared clinical and chemotherapeutic response profiles led us to hypothesize that these morphologically heterogeneous cancers share an underlying biology. In parallel, we had observed that

[1]Department of Genitourinary Medical Oncology, The University of Texas MD Anderson Cancer Center, Houston, Texas. [2]Department of Bioinformatics and Computational Biology, The University of Texas MD Anderson Cancer Center, Houston, Texas. [3]Department of Biostatistics, The University of Texas MD Anderson Cancer Center, Houston, Texas. [4]Department of Pathology, The University of Texas MD Anderson Cancer Center, Houston, Texas. [5]Human and Molecular Genetics Program, The University of Texas Graduate School of Biomedical Sciences, Houston, Texas. [6]Clinical and Translational Sciences Graduate Program, The University of Texas Graduate School of Biomedical Sciences, Houston, Texas.

Note: Supplementary data for this article are available at Clinical Cancer Research Online (http://clincancerres.aacrjournals.org/).

Corresponding Author: Ana M. Aparicio, Department of Genitourinary Medical Oncology, Unit 1374, The University of Texas MD Anderson Cancer Center, 1155 Pressler St., Houston, TX 77230-3721. Phone: 713-563-6969; Fax: 713-745-1625; E-mail: aaparicio@mdanderson.org

doi: 10.1158/1078-0432.CCR-15-1259

AACR

Translational Relevance

Prostate cancer is a heterogeneous disease yet available therapies continue to be applied homogeneously. Biomarkers that identify the clinically meaningful, therapeutically relevant prostate cancer subsets are needed to allow for optimal therapy development. Here we show that the aggressive variant prostate cancer (AVPC), a clinically defined subset of the disease that shares virulent and atypical clinical features and chemotherapy sensitivity with the small-cell prostate carcinomas (SCPC), are morphologically heterogeneous but can be identified by common molecular features (also shared with SCPC) and should be considered as a distinct clinical–biologic subset of prostate cancer with therapeutic implications. A candidate molecular signature consisting of joined alterations in RB1, Tp53, and/or PTEN is proposed which may account for the shared clinical features, resistance to AR inhibition and chemotherapy sensitivity and should serve as the foundation for a biologically defined therapeutically relevant classification of prostate cancer.

PDXs generated from cancers of men meeting AVPC criteria were frequently AR-negative and bore alterations in tumor suppressors, as well as increases in the expression of mitotic genes and proneural transcription factors (in line with others' observations; refs. 10–13). Here we combined our findings in PDX models with the clinically annotated NCT00514540 tumor tissues to more completely characterize AVPC and to identify markers of their underlying biology that can be deployed clinically to predict and prognosticate.

Materials and Methods

Patient tumor samples

We collected all available specimens stored in the MD Anderson Department of Pathology from patients registered ($n = 121$) to the clinical trial, a phase II study of carboplatin plus docetaxel in patients with anaplastic prostate carcinoma (NCT00514540). To be eligible, men with metastatic castration–resistant prostate cancer (mCRPC) had to display $\geq$1 of the "anaplastic" or AVPC eligibility criteria (Supplementary Table S1; ref. 9). Institutional review board (IRB)-approved written consent was obtained from participants before enrollment for the collection, banking, and use of tumor samples in research. IRB approval was obtained separately for the analyses described here.

A total of 114 patients were eligible for the NCT00514540 clinical trial. One patient was ineligible for treatment on trial due to thrombocytopenia but otherwise met AVPC criteria thus making 115 patients evaluable for the current study. We identified 70 surgically excised and biopsy specimens from 47 of the 115 evaluable patients. Of these, 59 (from 40 patients) had sufficient tumor to attempt a full immunohistochemical (IHC) panel (Table 1).

PDXs

We also used 8 PDX lines derived from 6 of the NCT00514540 trial participants (Supplementary Tables S2 and S3). MDA prostate cancer (PCa) 155-2, 144-4, and 144-13 have been reported previously (10). The latter two were derived from the same donor tumor. MDA PCa 177-0 and MDA PCa 189-1 were derived from the prostate of patient #83 −0.1 months before and 11.9 months after chemotherapy, respectively. Two (MDA PCa 163-A and MDA PCa 177-0) were obtained before chemotherapy and MDA PCa 163-A was obtained while patient had noncastrate levels of testosterone. The rest were obtained >5 months after the start of chemotherapy (timeline shown in Fig. 4). The donor tumors for MDA PCa 177-0, 189-1, and 166-1 were not available for study.

DNA extraction-Oncoscan

Tumor areas within samples were marked by the pathologist on a hematoxylin–eosin (H&E)-stained slide to guide the acquisition of a 0.6 mm core biopsy from the FFPE block. After xylene extraction and ethanol wash, DNA was isolated using the Recover All Total Nucleic Acid Isolation kit for FFPE (Life Technologies, catalog-AM1975). The average DNA recovered was 36.6 ng/mL (range, 2.6–203.3 ng/mL). All samples (de-identified) were placed on sealed 96-well plates provided by Affymetrix (as per Affymetrix Services Guide for Oncoscan FFPE Assay Kit) and shipped on dry ice.

IHC, quantitative real-time reverse transcriptase-PCR and Western blot analyses are described in Supplementary Material. Supplementary Tables S4 and S5 list the antibodies and primer sequences used.

Statistical analyses

Supervised hierarchical clustering of gene expression profiles. Gene expression of 6 PDX profiled using the U133A2.0 Plus array (Affymetrix, Inc.) was previously described. (11) Here, genes within categories of interest (luminal-epithelial-androgen, neural development, and cell-cycle-proliferation; Supplementary Fig. S1) were selected from RMA-processed and log2-transformed gene expression data to cluster samples with use of Euclidean distance and complete linkage.

Analyses of patient characteristics and IHC studies. Patient characteristics were tabulated by donor status. Fisher exact tests and Wilcoxon rank sum tests were used to test differences between covariates. Uncertain values of serum markers were replaced by their upper limits (for example, <0.1 was replaced by 0.1). The standardized ChrA was redefined as (ChrA-36.4)/36.4 or (ChrA-s - 225)/225. Relationships among the markers in donor patients were evaluated using Pearson correlations. A corrgram was applied for exploratory visual display (14).

The effect of the markers on variance was investigated using Principal component analysis (PCA) and component scores were grouped as $\geq$0 vs. <0. The association between component score groups and SCPC, overall survival (OS), or progression-free survival (PFS) were investigated by using Fisher test or log-rank tests, respectively. Cox proportional hazards regression models were fit to assess the association between AVPC markers and OS or PFS (15). Predictive factors were transformed as appropriate based on martingale residual plots (16). Statistical analyses were performed with SAS 9.3 (17) and S-Plus (18) software.

Bioinformatics analyses

Reports and detailed descriptions of the bioinformatics analyses performed in this study are available on the UT MDACC

Department of Bioinformatics and Computational Biology website http://bioinformatics.mdanderson.org/main/Publications_Supplements_Data. Data for 44 (36 prostate cancer patient samples; 8 PDX samples) plus 2 Affymetrix control samples were submitted producing 92 CEL files (two arrays per sample: AT and GC channels) and have been deposited in the Gene Expression Omnibus (GEO) under accession number GSE73902. Raw data were processed in Affymetrix OncoScan Console to yield log R ratios (LRR) and B allele frequencies (BAF) for each single nucleotide polymorphism (SNP) in each sample by using the TuScan algorithm. Computations were performed relative to the normal reference provided by Affymetrix. LRR and BAF plots were generated along each chromosome for each sample with use of ASCAT 2.1 (allele-specific copy number analysis of tumors, version 2.1). Two quality control (QC) metrics provided by the software, the MAPD (median of the absolute values of all pairwise differences) and the ndSNPQC (SNP QC of Normal Diploid Markers) were within bounds in 23 (52.3%) and 18 (40.9%) of the 44 samples, respectively. Given that these QC markers were developed for normal diploid genomes and that heterogeneous tumor samples are expected to diverge from these, we used all available data in our analyses.

We queried the segmentations in regions corresponding to genes according to hg19-RefSeq Transcript coordinates. To make copy number calls for each gene and distinguish focal from broad-based changes, we used LRR values relative to (a) absolute cutoffs and (b) the median segmentation of the corresponding chromosome arm (p or q). For regions with multiple segments, the extreme value away from zero was used to make the copy number call. To determine how gene-specific events related to regional/chromosomal integrity, we plotted the LRR values for each gene of interest versus the LRR values for the corresponding chromosomal arm. To study the correlation between copy number (median of segmentation) and labeling indices, we performed both Pearson and Spearman analyses. The Broad Institute GISTIC 2.0 tool was used for clustering of the median LRR values for each chromosome arm.

We used both unsupervised (PCA) and supervised display methods to determine the degree to which the AVPC samples stood out from the unselected TCGA prostate cancer population. These analyses used level 3 copy number estimates from Affymetrix SNP6 arrays ($n = 404$) and somatic mutation calls for Tp53 retrieved from cBioPortal ($n = 253$ of the 404; refs. 19, 20). To define our final classification rule, we used logistic regression with 10 potential exploratory covariates and used top-forward regression coupled with cross-validation to arrive at a solution with high sensitivity. Copy number alterations and Tp53 mutations within the data reported by Robinson and colleagues (21) were queried from cBio.

Results

Interactions between tumor suppressors, AR-signaling, neurodevelopmental and mitotic immunohistochemistry, and serum markers in the AVPC

In our previously reported PDX gene expression profile (11), we found that SCPCs segregated from typical CRPC adenocarcinomas based on RB loss and expression of luminal epithelial markers, genes implicated in mitosis and proneural transcription factors (Supplementary Fig. S1). We also found (as others) frequent Tp53 alterations in the SCPCs (10, 13). To examine whether the clinically defined AVPC shared molecular features with SCPC, we used IHC analysis to query the expression of RB1, Tp53, AR, NKX3-1, ASCL1, BRN2, AURKA, UBE2C, and Ki67 in the 59 tumor samples and 8 PDX lines obtained from 42 participants in clinical trial NCT00514540 for men with mCRPC meeting AVPC criteria (Supplementary Table S1; ref. 9). Of the 59 samples (Table 1), 5 from 5 patients (early) were obtained >13 months prior to registration (median 24.1; range −131.6 to −14.0); 38 from 31 patients (baseline) between −13 and +1 months from registration (median −0.18; range −12.18 to +1), and 16 from 13 patients (postchemotherapy) >1 month after registration and chemotherapy (median 7.43; range 4.04 to 28.46). Supplementary Tables S6 and S7 summarize the patient donor characteristics and serum marker levels at registration. Supplementary Figure S2 shows their morphologic spectrum. The 31 patient donors of the "Baseline samples" were similar to "nondonor" participants of the NCT00514540 trial except for having worse Eastern Cooperative Oncology Group (ECOG) Performance Status (PS) scores ($P < 0.001$) and higher lactate dehydrogenase ($P < 0.001$) levels. Supplementary Tables S2 and S3 summarize the clinicopathologic features of the donor patients and tumors for the PDX, their growth rates and their PSA production.

Shown in Fig. 1A are the percent of cells with positive stains for each marker in the "Baseline samples." Where repeated measurements were available for a single patient, only the measurement taken closest to the registration date was considered ($n = 31$). Of these 80.6% (25/31) displayed Ki67 labeling indices ≥10%, as did 71.0% (22/31) for nuclear (-N) AURKA (AURKA-N), 51.6% (16/31) for cytoplasmic (-C) AURKA (AURKA-C), 35.5% (11/31) for both AURKA-N and AURKA-C, 44.8% (13/29, 2 uninterpretable) for UBE2C-N, 48.3% (14/29) for UBE2C-C, 37.9% (11/29) for both UBE2C-N and UBE2C-C, and 32.2% (10/31) for Tp53. In 62.1% (18/29, 2 uninterpretable) and 41.9% (13/31) RB1 and AR stained <10% nuclei, respectively. Results for the remaining samples are in Supplementary Fig. S3.

RB1-negative samples appeared more likely to be AR-negative, to be Tp53-positive, and to have higher Ki67 and UBE2C staining. Indeed, Pearson correlations of the 10 tissue markers of the "Baseline samples" and the levels of 6 serum markers at registration (PSA, PAP, CEA, chromogranin A, calcitonin, and somatostatin; Fig. 1B; Table 2) showed strong positive correlations between AR and NKX3.1, RB1, AURKA-N, and serum PSA. Strong positive correlations were also observed between NKX3.1 and RB1; Tp53 and UBE2C-N and Ki67; UBE2C-N and Ki67 and serum somatostatin; UBE2C-C and Ki67; and PSA and calcitonin. A strong negative correlation was observed between NKX3.1 and Ki67.

To determine which marker(s) best explained the variance in the data and examine their relationship with outcome, PCA was applied to the 16 serum and IHC tumor marker set of the "Baseline" samples from 21 patients (10/31 were excluded due to missing values). The first principal component had high positive correlations with PSA, AR-N, NKX3.1-N, RB1, and AURKA-N, and negative correlations with Tp53, UBE2C-N, Ki67, and somatostatin (Supplementary Fig. S4A). A strong association between small cell morphology ($n = 6$ samples) and first component score ≥0 versus <0 was observed ($P = 0.01$), but clustering of the samples was not (Supplementary Fig. S4B). Neither overall survival (OS) nor progression-free survival (PFS) were

Table 1. Data structure: description of samples used in reported analyses

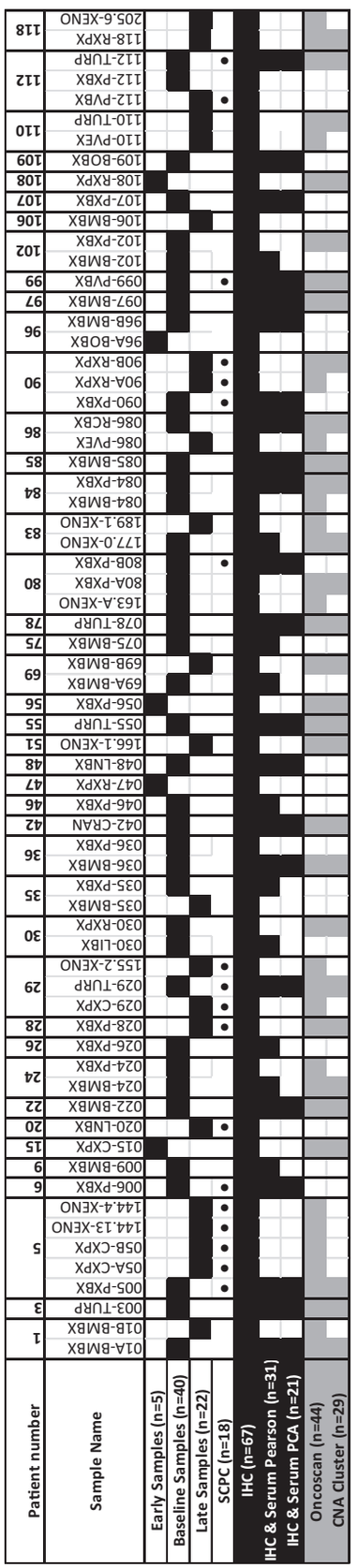

Sample names indicate patient or PDX line number and the procedure and site of origin. Samples are ordered by patient. Early samples were obtained more than 13 months prior to registration to NCT00514540. Baseline samples were obtained between −13 and +1 months from registration. Late samples were obtained >1 month after registration and after chemotherapy. Abbreviations: BMBX: bone marrow biopsy; TURP: transurethral resection of prostate; PXBX: prostate biopsy; CXPX: cystoprostatectomy; XENO: xenograft; LNBX: lymph node biopsy; LIBX: liver biopsy; RXPX: radical prostatectomy; CRAN: craniotomy; PVEX: pelvic exenteration; RCBX: rectal biopsy; BOBX: bone biopsy; PVBX: pelvic mass biopsy SCPC, small cell prostate carcinoma; IHC, immunohistochemistry; PCA, principal component analysis; CNA, copy number alteration.

significantly associated with the dichotomized first component scores within this sample set (data not shown).

These data suggest that, irrespective of morphology, AVPCs express high levels of mitotic markers, are frequently RB1 negative and that RB1 loss within them is often associated with mutant Tp53, loss of AR, and high Ki67. The observed heterogeneity may be due to limitations in the specificity of the clinical criteria used for patient selection, to the shortcomings of IHC analysis of a single marker to evaluate a full pathway, and/or to actual biologic heterogeneity within AVPC.

Copy number alterations in AVPCs

Absence of a full-length RB1 protein in SCPC is commonly a consequence of genomic deletions or microdeletions in *RB1* (11, 13). The mechanisms of Tp53 alteration are more diverse and include gene mutations or deletions (13). Also, *AURKA* amplification has been reported in 40% of SCPC, with concurrent *MYCN* amplification (12). To expand on the IHC findings and further investigate the potential heterogeneity within the AVPCs, we submitted DNA from 44 tumor samples (36 patient samples and 8 PDXs) for Oncoscan analysis.

Assuming 60% tumor purity and using absolute cut-off values, a total of 197,971 copy number alteration (CNA) calls (58,845 losses and 139,126 gains) were made across all samples; 22,279 of 22,355 genes (99.7%) displayed $\geq$1 CNA in $\geq$1 sample. However, tumor samples varied widely with respect to CNA: between 29 and 17,249 (median 3,650.5) CNA calls made per sample (Supplementary Fig. S5, full list at http://bioinformatics.mdanderson.org/main/Publications_Supplements_Data).

The gene showing the highest CNA rate across the AVPC tumors was *ADCY8* (8q24.22), amplified in 27 of 44 samples (61.4%). *MYC* (8q24.21) was amplified in 24 (54.5%). The gene that showed the highest rate of copy number loss (CNL) was *RB1* (13q14.2), lost in 24 samples (54.5%), followed by *PTEN* (10q23.31), lost in 21 (47.7%). Also using absolute cut-off values, copy number gains (CNG) were called for *AURKA* (20q13.31) in 11 samples (25.0%), *MYCN* (2p24.3), *UBE2C* (20q13.12) and *AR* (Xq12) in 9 (20.4%) each, and *ASCL1* (12q23.2) in 6 (13.6%). CNL for *NKX3-1* (8p21.2) were called in 14 samples (31.8%) and for *Tp53* (17p13.1) in 11 (25.0%). Seven samples (15.9%) from 5 patients displayed concurrent *AURKA* and *MYCN* CNG, 4 of which (from 2 patients) showed SCPC morphology.

Because a CNA that involves a specific gene segment (as opposed to a region containing multiple genes) reinforces the functional significance of the gene we used cut-off values relative to the corresponding chromosome arm to ask whether the CNA involving each of the genes of interest was a "segmental" versus a "regional" alteration. As shown in Fig. 2A, 19/21 samples showed CNL for *PTEN* despite copy number neutral values for the median of the chromosome arm 10q, suggesting a gene-specific alteration. This was also true for *RB1* in 11 of the 24 samples with CNL and for *MYCN* in 4 of 9 samples with CNG. However, for *Tp53* and *AURKA* the number of CNA calls using the relative cut-off values decreased to 2 (1 loss and 1 gain for both) and for *MYC* to 0.

We examined the correlation between the IHC labeling indices and copy number for each marker. *RB1* CNA showed a positive correlation with its labeling index (Fig. 2B) but a number of copy number neutral tumors showed $\leq$10% RB1-positive cells, indicating CNL is not the sole mechanism of RB silencing in these

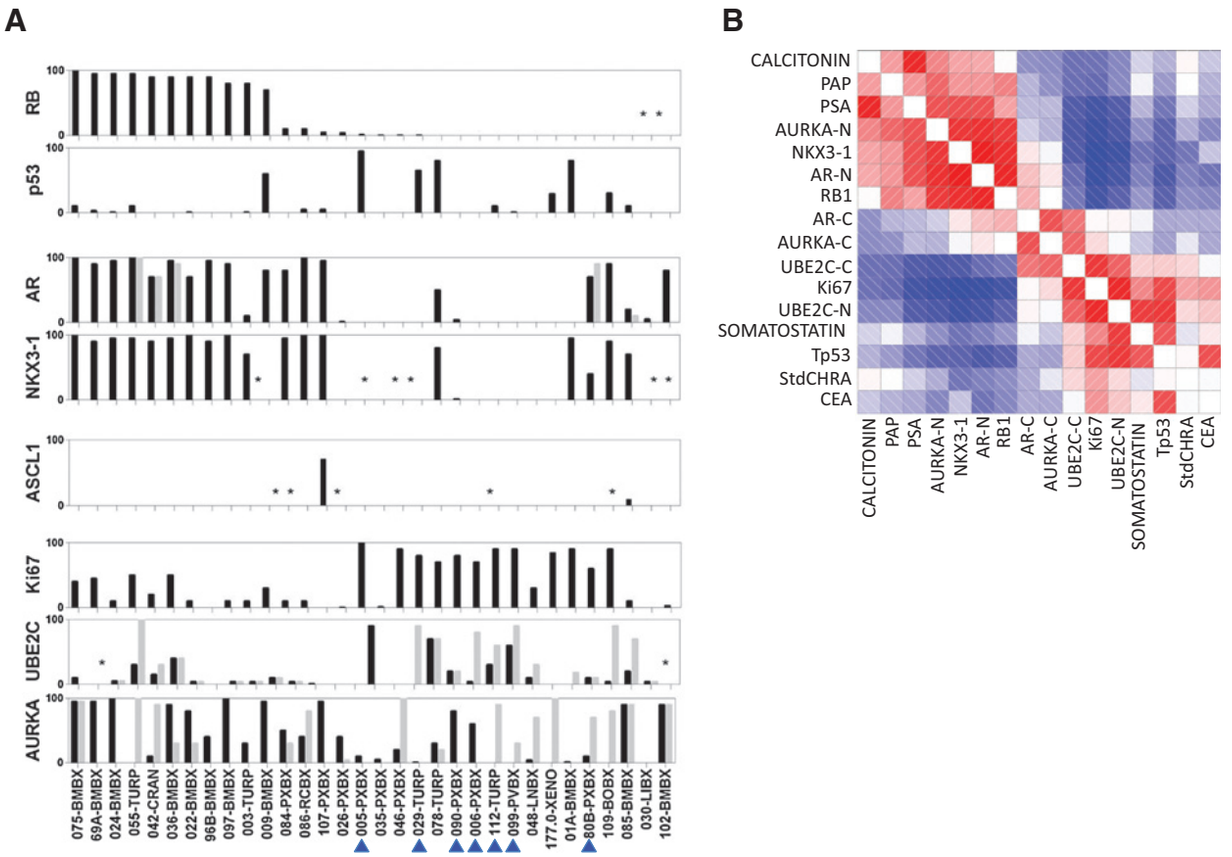

Figure 1.

IHC analysis of NCT00514540 unique "Baseline" samples. A, labeling indices (% of cells staining positive for the marker listed on the *y*-axis, Li) for RB1, Tp53, AR, NKX3-1, AURKA, UBE2C, and Ki67 in unique patient and PDX baseline samples (only one sample per patient is shown of the set obtained between −13 and +1 months from registration). Note, 177-0-XENO is included in the graph ($n = 32$) but not in the analyses described in the text because the donor-patient tumor was not available for analysis. The BRN2 stains did not work and are not reported. Black bars depict nuclear staining. For AR, AURKA, and UBE2C cytoplasmic stains are shown in light gray. Each individual sample is listed on the *x*-axis. Numbers indicate accession number on the protocol or PDX line. Letters indicate site of origin. Blue arrowheads indicate SCPC morphology. B, Corrgram of selected tissue and serum markers among the 31 baseline samples' donors. Red represents positive values and blue represents negative values. The intensity of the color is proportional to the magnitude of the correlation. Asterisk (*) indicates the IHC did not work. Abbreviations: RB, retinoblastoma 1; p53, tumor suppressor Tp53; NKX3-1, NK3 homeobox 1; AURKA, aurora kinase A; UBE2C, ubiquitin conjugating enzyme 2C; Ki67, antigen identified by monoclonal antibody Ki-67; RXPX, radical prostatectomy; BMBX, bone marrow biopsy; TURP, transurethral resection of prostate; CRAN, craniotomy; RCBX, rectal biopsy; XENO, xenograft; PVBX, pelvic mass biopsy; LNBX, lymph node biopsy; BOBX, bone biopsy; LIBX, liver biopsy; PAP, prostatic acid phosphatase; PSA, prostate-specific antigen; -N, nuclear staining; -C, cytoplasmic staining; StdCHRA, standardized chromogranin A; CEA, carcinoembryonic antigen.

tumors. For the remaining markers, there was no correlation between CNA and their labeling indices (data not shown).

These data indicate that the most common CNA across the AVPC samples are 8q amplification and RB1 and PTEN CNL (which occurred irrespective of morphology, i.e., in both small-cell and non–small cell histologies alike), and also that CNA are insufficient to detect full pathway alterations in these tumor samples (12, 22).

Pathway analysis in PDX

To gain insight into the significance and the functional consequences of the alterations observed by IHC and copy number analysis, we examined associated and downstream molecular events in the PDX models.

Loss of RB1 RNA and protein expression was a frequent finding, consistent with the CNL observations (Fig. 3). Two of the 3 RB-positive PDX showed high levels of phosphor-RB by Western blot analysis, an inactive RB state (23). We interrogated levels of representative genes from published RB-loss signatures (24), by qRT-PCR (Supplementary Fig. S6A). In all but one (MDA PCa 163A) of the RB-negative and hyperphosphorylated RB PDX, this partial RB-loss signature was expressed at intermediate to high levels relative to the RB-positive PDX MDA PCa 189-1.

We found Tp53 mutations in 7 of the 8 PDX lines, 6 of them within the DNA-binding domain (Fig. 3). In MDA PCa 163-A, a truncating mutation (R65*) was associated with loss of expression, exemplifying the fact that absent Tp53 staining does not signify an intact gene and suggesting that Tp53 alterations are more common in the AVPC samples than was evident by IHC analysis. At least two of the Tp53 mutants found (R273C and Y163N) have been associated with gain-of-function activity (25, 26). Whether distinct Tp53 mutants are linked to different clinical phenotypes remains to be determined.

Table 2. Correlations between selected measurements of tissue and serum markers among "baseline samples" ($n = 31$)

	CALCITONIN	PAP	PSA	AURKA-N	NKX3-1	AR-N	RB1	AR-C	AURKA-C	UBE2C-C	Ki67	UBE2C-N	SOMATOSTATIN	Tp53	StdCHRA	CEA
CALCITONIN	1	0.21	0.68	0.24	0.15	0.19	−0.14	−0.08	−0.19	−0.14	−0.20	−0.09	0.03	−0.04	0.10	−0.04
PAP	0.21	1	0.12	0.27	0.17	0.22	0.28	−0.07	−0.16	−0.13	−0.17	−0.09	0.19	−0.11	0.11	−0.05
PSA	0.68	0.12	1	0.28	0.44	0.50	0.01	−0.11	−0.10	−0.31	−0.43	−0.25	0.06	−0.21	−0.01	−0.12
AURKA-N	0.24	0.27	0.28	1	0.43	0.51	0.47	−0.15	−0.18	−0.34	−0.42	−0.28	−0.10	−0.25	−0.12	−0.23
NKX3-1	0.15	0.17	0.44	0.43	1	0.82	0.59	0.17	0.10	−0.40	−0.61	−0.49	−0.19	−0.17	−0.30	0.13
AR-N	0.19	0.22	0.50	0.51	0.82	1	0.64	0.33	0.20	−0.11	−0.38	−0.22	−0.05	−0.20	−0.15	−0.23
RB1	−0.14	0.28	0.01	0.47	0.59	0.64	1	0.30	−0.03	−0.21	−0.42	−0.13	−0.07	−0.27	−0.13	−0.17
AR-C	−0.08	−0.07	−0.11	−0.15	0.17	0.33	0.30	1	0.37	0.45	0.06	0.13	0.13	−0.17	−0.12	−0.08
AURKA-C	−0.19	−0.16	−0.10	−0.18	0.10	0.20	−0.03	0.37	1	0.41	0.12	−0.02	−0.06	−0.24	−0.03	−0.17
UBE2C-C	−0.14	−0.13	−0.31	−0.34	−0.40	−0.11	−0.21	0.45	0.41	1	0.65	0.34	0.00	−0.05	−0.01	−0.10
Ki67	−0.20	−0.17	−0.43	−0.42	−0.61	−0.38	−0.42	0.06	0.12	0.65	1	0.60	0.25	0.51	0.27	0.29
UBE2C-N	−0.09	−0.09	−0.25	−0.28	−0.49	−0.22	−0.13	0.13	−0.02	0.34	0.60	1	0.56	0.57	0.03	−0.01
SOMATOSTATIN	0.03	0.19	0.06	−0.10	−0.19	−0.05	−0.07	0.13	−0.06	0.00	0.25	0.56	1	0.41	−0.12	−0.03
Tp53	−0.04	−0.11	−0.21	−0.25	−0.17	−0.20	−0.27	−0.17	−0.24	−0.05	0.51	0.57	0.41	1	−0.08	0.47
StdCHRA	0.10	0.11	−0.01	−0.12	−0.30	−0.15	−0.13	−0.12	−0.03	−0.01	0.27	0.03	−0.12	−0.08	1	−0.05
CEA	−0.04	−0.05	−0.12	−0.23	0.13	−0.23	−0.17	−0.08	−0.17	−0.10	0.29	−0.01	−0.03	0.47	−0.05	1

NOTE: Strong correlations (≥0.5) are highlighted in black. Abbreviations are described in the Fig. 1B legend.

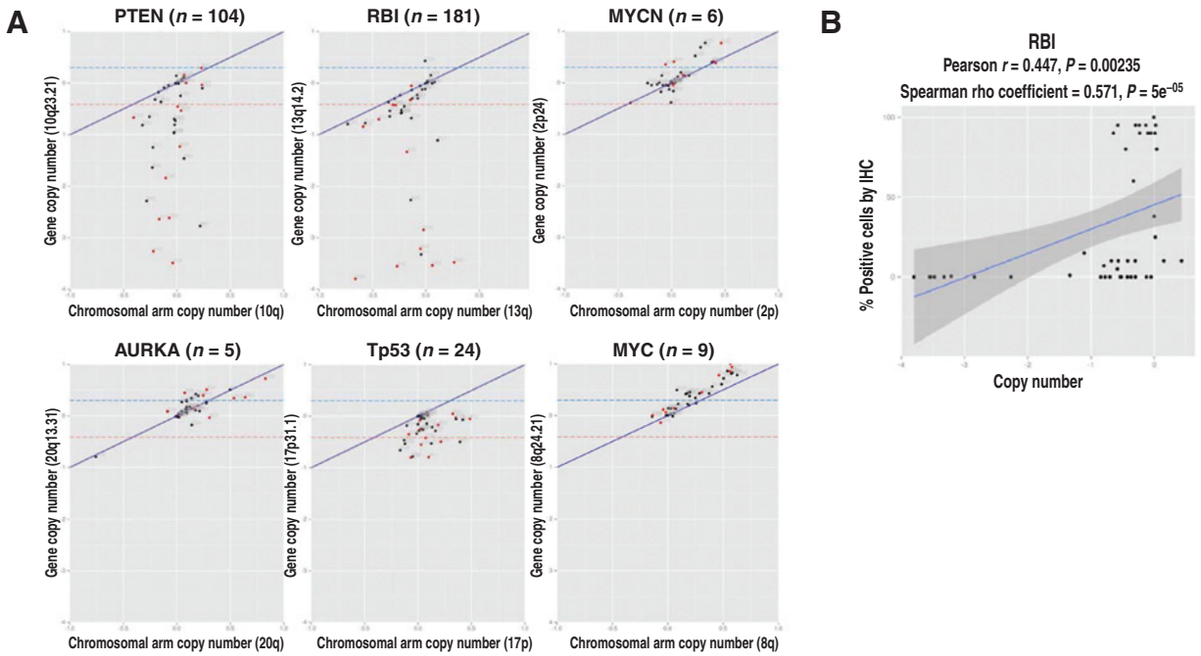

Figure 2.

Copy number alterations at genes of interest and correlation with IHC results. A, segmental (values corresponding only to the gene of interest) versus regional (median values for the corresponding chromosome arm) copy number calls for *PTEN*, *RB1*, *MYCN*, *AURKA*, *Tp53*, and *MYC*. "n" in parenthesis following the gene name indicates the number of gene-specific probes present on the Oncoscan chip. The blue and red dashed lines indicate the absolute cutoff values. The solid blue line represents the corresponding chromosome arm copy number. Red dots indicate samples with SCPC morphology. B, correlation between labeling indices (*y*-axis) and copy number (*x*-axis) for *RB1*.

As in the patient samples, AR expression was heterogeneous in the PDX and its presence tightly associated with canonical downstream signaling markers (such as PSA) and markers of luminal epithelial differentiation (such as HOXB13 and the pioneer factor GATA2; Supplementary Fig. S6B). NKX3-1 and FOXA1 were expressed in all AR-positive tumors but also in some of the AR-negative tumors. These data suggest that, when AR is expressed it remains active and within the context of a prostate luminal epithelial program. AR splice variants were also expressed in the AR-positive tumors but at much lower levels than the full-length AR.

An inverse correlation between the expression of AR and that of the proneural transcription factors (TF) tested (ASCL1, BRN2, NEUROD1, INSM1, MYCN) was observed (Fig. 3 and Supplementary Fig. S6C). However, there was no single proneural TF that showed increased expression across all models. Even within PDX lines derived from the same tumor, MDA PCa 144-13 and MDA PCa 144-4 (10), the expression of proneural TF was heterogeneous. REST was absent in the PDX lines with small cell carcinoma morphology, which had the highest levels of proneural TF. However, in MDA PCa 177-0, BRN2 and MYCN were expressed despite the presence of REST (Supplementary Fig. S6C). These findings are consistent with the hypothesis that neural developmental pathways are coopted in the latter stages of tumor evolution. They also suggest that, as in neural development, different combinations of proneural TF result in distinct corresponding functions and account for the increased migratory and invasive promiscuity that is reflected in the unconstrained metastatic patterns of AVPC.

Levels of AURKA mRNA were concordant with those of UBE2C while levels of AURKB mRNA for the most part paralleled those of PLK1 and were higher in the AR-negative PDX (Supplementary Fig. S6D). Protein levels of all three mitotic kinases and UBE2C were lowest in MDA PCa 205-6 and MDA PCa 189-2. MDA PCa 205-6 was derived from sample 118-RXPX (Supplementary Fig. S3), which was donated by the patient with the longest survival (Supplementary Table S2) of the PDX donors. It was also the only PDX in which a Tp53 mutation was not found. MDA PCa 189-1 was derived, after chemotherapy, from the same patient as MDA PCa 177-0. Both PDX retained the Y163N Tp53 mutation but while the prechemotherapy MDA PCa 177-0 PDX was RB-negative/AR-negative/proneural TF-positive high, the postchemotherapy MDA PCa 189-1 was RB-positive/AR-positive/proneural TF-negative and expressed lower levels of Tp53, suggesting either clonal selection or tumor plasticity as a result of treatment. Protein and mRNA levels of the mitotic kinases and UBE2C were not correlated, corroborating the importance of regulatory posttranslational events for these markers.

Integration of IHC, CNA, and PDX data and refinement of marker selection with reference to publicly available datasets

With the overall goal of arriving at a candidate molecular signature to distinguish the AVPC and guide therapy allocation in men with CRPC, we combined the IHC, CNA, and PDX data and used The Cancer Genome Atlas (TCGA) and a recently published unselected CRPC dataset (21) to refine our marker selection.

We examined the rate of CNA in the genes of the markers initially queried by IHC (RB1, Tp53, AR, NKX3-1, ASCL1, AURKA, and UBE2C) in the 404 samples from TCGA analyzed by Affymetrix SNP 6.0 Array and the 150 unselected CRPC

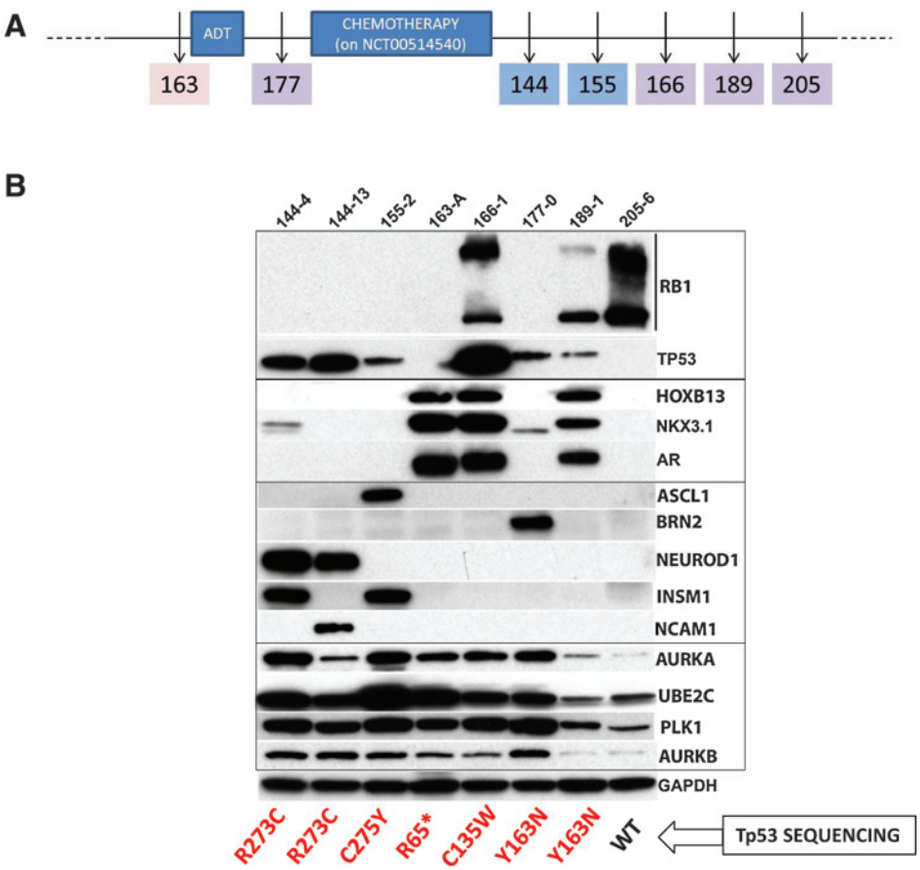

Figure 3.
Analyses in PDX. A, PDX development relative to start of ADT and chemotherapy. Numbers indicate PDX line. The MDA-PCa 163 PDX line was derived from the prostate tumor of patient #80 on NCT00514540 in the non-castrate setting (pink shaded box). Blue shade indicates SCPC morphology. Purple shade indicates castration-resistant prostate tumor without SCPC morphology. B, Western blot analyses of markers of interest and Tp53 mutations (shown in red) in PDX. Abbreviations: PDX, patient-tumor derived xenograft; ADT, androgen deprivation therapy; WT, wild-type.

samples recently reported by Robinson and colleagues (21) We also queried *PTEN* and *MYC* (the latter taken as a surrogate for 8q amplification), given their frequent alteration in the AVPC samples, as well as *MYCN*, given its reported frequent amplification in SCPC (12), and Repressor element (RE)-1 silencing transcription factor (*REST*), given its role as a master transcriptional regulator of neural development and its reported down-regulation in SCPC (ref. 22; Fig. 4A). An unsupervised PCA (Supplementary Fig. S7) showed that of the 10-CNA-marker(s) (*RB1*, *PTEN*, *Tp53*, *MYC*, *MYCN*, *NKX3-1*, *ASCL1*, *REST*, *AURKA*, and *UBE2C*) MYC and NKX3-1 best explained the variance between the three sample sets (Supplementary Table S8). As our primary objective is to identify the AVPC within an unselected CRPC population, we applied a supervised linear discriminant analysis to examine the segregating ability of the 10-CNA marker (Fig. 4B). In this analysis, 38 (25.3%) of the 150 unselected CRPC samples segregated with the AVPC samples (an expected proportion based on our prior experience) and RB1 CNL carried the largest weight in this distinction (Supplementary Table S9).

Hence alterations in RB1 (both CNL and/or negative staining by IHC), Tp53 (CNL, positive staining by IHC and/or detectable mutation), PTEN CNL, and MYC CNG appeared to be the most common molecular alterations of the AVPC, with MYC CNG seemingly more frequent in the unselected CRPC than in the AVPC. These are prevalent alterations in CRPC (21, 27), and have been described at various rates in primary prostate tumors (27), but genetically engineered mouse models (GEMM) have shown that each of these alterations individually is insufficient to result in lethal prostate cancer (28–32). In contrast, the concurrent loss of RB1 and Tp53 resulted in highly metastatic neoplasms of various morphologies that are resistant to androgen depletion from early stages of development both in Tag, TRAMP, and PB-Cre4 (*PB-Cre4*,$p53^{loxP/loxP}$,$Rb^{loxP/loxP}$) driven models (33, 34) and haploinsufficiency of the *Pten* gene increased the rates of tumor progression in the TRAMP mouse model (35).

We thus asked how often the alterations in RB1, Tp53, and PTEN occurred together in TCGA, the AVPC and the unselected CRPC samples (21) using the available information. Here we included Tp53 mutations identified by sequencing in the unselected CRPC and TCGA samples (70 (46.7%) of 150 and 24 (9.5%) of 253, respectively (Supplementary Table S10). In the AVPC samples, Tp53 sequencing was only available for the PDX and high confidence calls using the Oncoscan data could only be made for 3 of the 29 samples (therefore, here the rate of Tp53 mutations in the AVPC is underestimated). Alterations in $\geq$2 of the 3 markers were found in 25 (9.9%) of the 253 TCGA samples for which Tp53 mutation status was available, in 39 (26.0%) of the 150 unselected CRPC and in 14 (48.3%) of the 29 AVPC samples.

Taken together, our observations in patient tumors and PDX models suggest that, irrespective of morphology, clinically defined AVPC are characterized by joint alterations in two or more of the following: RB1, Tp53, and PTEN.

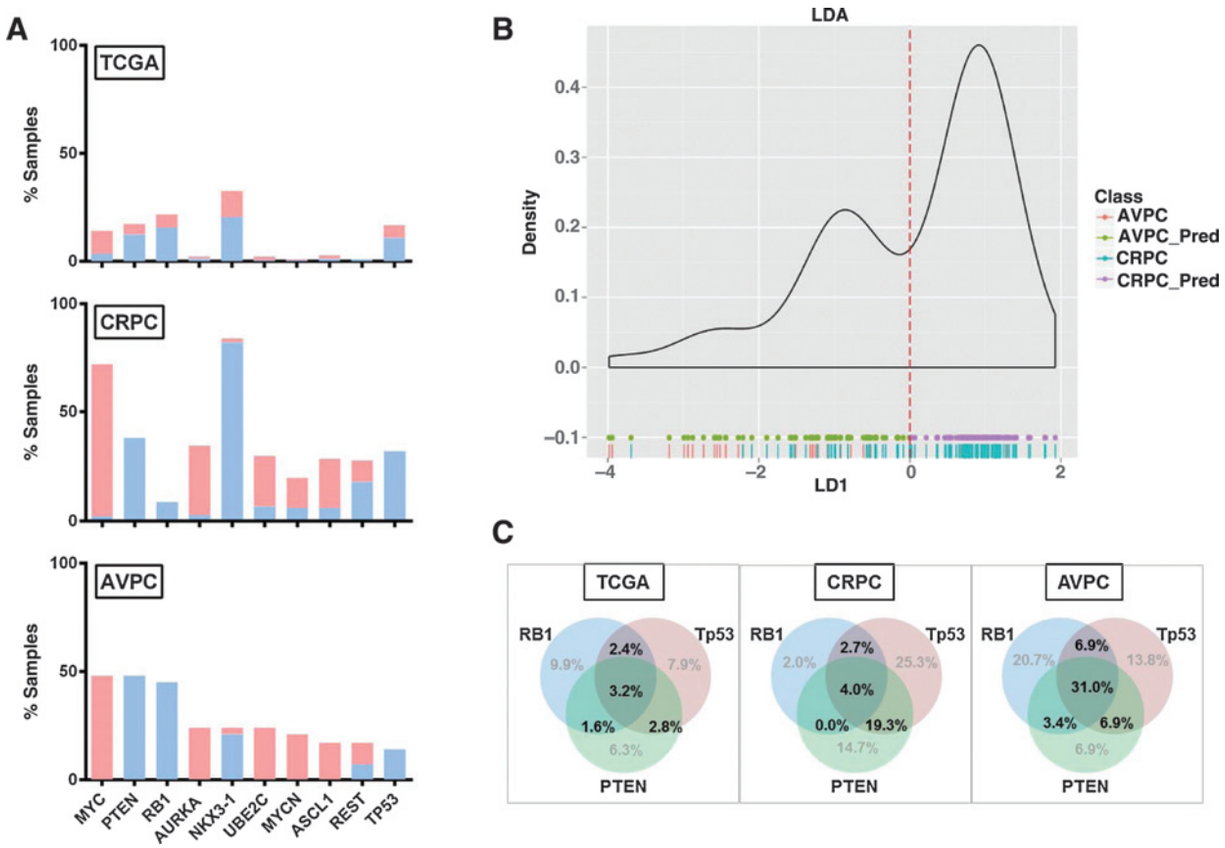

Figure 4.
AVPC data with reference to publicly available TCGA and unselected CRPC datasets. A, histograms showing percentage of samples with CNA (per absolute cut-offs) at segments corresponding to genes of interest in TCGA, unselected CRPC (middle) and AVPC 7. In blue are copy number losses and in red are copy number gains. B, linear discriminant analysis of AVPC and unselected CRPC samples using the 10 CNA marker set. Green and purple dots at the bottom indicate predicted AVPC (AVPC_Pred) and non-AVPC (CRPC_Pred) predictions, respectively, while red and blue vertical lines indicate actual AVPC and unselected CRPC samples, respectively. C, Venn diagrams showing the rates of combined RB1, Tp53, and/or PTEN alterations in the TCGA ($n = 253$), CRPC ($n = 150$), and AVPC ($n = 29$) samples.

Discussion

The findings we report link the prospectively clinically defined AVPC and their corresponding PDX to a molecular marker profile not predicted by morphology and suggest that the aberrancy of multiple tumor suppressors (RB1, Tp53, and/or PTEN) is a dominant "driver" leading to the development of this phenotype. Whether different combinations of the alterations are linked to distinct clinical behaviors within the AVPC remains to be determined. Adding significance to the findings is the similarity of the molecular alterations to those observed in SCPC. Furthermore, these alterations have been linked to increased DNA damage response signaling (36) which, in a parallel study, we have identified in the AVPC (26), and may represent an actionable therapy target for this entity. The results from our dataset and those of others (12, 13, 22), will lead to the identification of predictive markers that enable the development and use of effective therapy combinations and sequences in the biologically distinct subsets of men with metastatic CRPC.

It has been proposed that *AURKA* amplification and overexpression are implicated in the pathogenesis of SCPC (12). We observed a high frequency of increased nuclear and/or cytoplasmic AURKA expression as well as 20q amplification in 7 (24.1%) of 29 unique AVPC samples irrespective of morphology. Intriguingly, in the AVPC, AURKA nuclear expression correlated with AR expression. Indeed, the interactome of AURKA is large (37) and includes cell cycle and transcriptional regulators such as AR (38), Tp53 (39), MYC (40), and BRCA1 (41). In turn, Tp53 mutants increase AURKA expression and cooperate with AURKA in the induction of genomic instability (ref. 42; also a likely feature of the AVPC suggested by the high rate of CNA observed) and in the regulation of DNA damage repair (43). Although these data are congruent with a role for AURKA in the pathogenesis of the AVPC, two concerns remain. First, amplification of AURKA is most often regional and thus accompanied by the enhanced expression of multiple additional genes, making the attribution of outcomes to AURKA overexpression alone difficult (37). Second, there is a lack of a standard IHC methodology and of a consensus as to what constitutes abnormal AURKA expression (37, 44). Thus, additional investigation is needed to determine the significance of AURKA expression in the AVPC and its value as a marker of this phenotype.

The loss of AR in a large proportion of the AVPC is consistent with the resistance to AR signaling inhibition. Of interest is

the finding that AR expression is inversely correlated with that of neurodevelopmental pathway markers. If confirmed, this observation would be in contrast to the frequent coexpression of AR with markers of neuroendocrine differentiation such as chromogranin A (45). The presence of neuroendocrine differentiation is often considered a precursor or even synonymous with SCPC. However, neuroendocrine marker expression in prostate tumors is associated with a wide range of clinical behaviors (46) and is not predictive of chemotherapy responsiveness (47). A master regulator of the neural-progenitor phenotype program or a consistent signature that reflects it remains to be fully characterized. Loss of REST has been proposed (22), although in our PDX models, the expression of proneural TF was not consistently linked to loss of REST mRNA. Experiments are ongoing to determine whether these sequences correspond to the known dominant-negative REST splice variant (48). Additional studies in larger numbers of patients will be needed to determine whether adoption of a neural-progenitor program is but one path of progression to the AVPC and whether this heterogeneity reflects clinically meaningful subsets within them. Although speculative, the loss of markers of androgen signaling and the transdifferentiation to a neural-progenitor phenotype are aligned with the resistance to androgen ablation and the multiorgan involvement that characterize the AVPC.

The parallel study of PDX allowed us to expand and gain confidence in our findings. For example, we confirmed that RB1 protein expression is not unequivocally linked to RB1 pathway integrity and were able to identify Tp53 mutations not detected by IHC or Oncoscan analysis. These observations will serve as the basis for the development of clinically applicable assays. An intriguing result was the different phenotype (RB-negative/AR-negative/Tp53/proneural TF-positive high vs. RB-positive/AR-positive/Tp53 low/proneural TF-negative) observed in the PDXs derived from patient #83 before and after chemotherapy. While this might simply be revealing of tissue sampling variability or clonal selection postchemotherapy, it could also be a reflection of tumor plasticity mediated by mechanisms such as chromatin modifications (49) or extrachromosomal DNA elimination (50).

The data we report demonstrate that some castration-resistant prostate adenocarcinomas share molecular as well as clinical features with SCPC. The consistent marker profile of the morphologically heterogeneous cancers in this dataset comprises combined alterations in RB1, Tp53, and/or PTEN. This marker profile can account for the observed cell-cycle alterations, AR signaling loss, and neural progenitor program adoption, which in turn can explain the clinical phenotype. Ongoing studies will determine the prevalence of AVPC, prospectively evaluate the utility of the proposed marker signature, characterize the potential heterogeneity within them, and test specific therapies tailored to their unique biology.

Disclosure of Potential Conflicts of Interest

No potential conflicts of interest were disclosed.

Authors' Contributions

Conception and design: A.M. Aparicio, S.N. Maity, C.J. Logothetis
Development of methodology: L. Shen, J.-F. Lu, S.N. Maity, A.M. Aparicio
Acquisition of data (provided animals, acquired and managed patients, provided facilities, etc.): A.M. Aparicio, E.L.N. Tapia, G. Wu, P. Troncoso, P. Corn, S.N. Maity
Analysis and interpretation of data (e.g., statistical analysis, biostatistics, computational analysis): A.M. Aparicio, L. Shen, H.-C. Chen, J. Zhang, X. Wang, P. Troncoso, P. Corn, B. Broom, K. Baggerly, S.N. Maity
Writing, review, and/or revision of the manuscript: A.M. Aparicio, L. Shen, E.L.N. Tapia, H.-C. Chen, J. Zhang, P. Troncoso, P. Corn, T.C. Thompson, B. Broom, S.N. Maity, C. Logothetis
Administrative, technical, or material support (i.e., reporting or organizing data, constructing databases): J.-F. Lu, C. Logothetis, A.M. Aparicio
Study supervision: A.M. Aparicio, S.N. Maity, C.J. Logothetis

Grant Support

This work was supported by the NIH/NCI [under award numbers P30CA016672 (Bioinformatics Shared Resource) and P50CA140388], the Prostate Cancer Foundation, the Joan Stanford Alexander Family Fund, the Michael and Susan Dell Foundation (honoring Lorraine Dell), and The University of Texas MD Anderson Prostate Cancer Moon Shot Program.

The costs of publication of this article were defrayed in part by the payment of page charges. This article must therefore be hereby marked *advertisement* in accordance with 18 U.S.C. Section 1734 solely to indicate this fact.

Received May 28, 2015; revised October 12, 2015; accepted October 25, 2015; published OnlineFirst November 6, 2015.

References

1. Jensen EV, Block GE, Smith S, Kyser K, DeSombre ER. Estrogen receptors and breast cancer response to adrenalectomy. Natl Cancer Inst Monogr 1971;34:55–70.
2. Slamon DJ, Clark GM, Wong SG, Levin WJ, Ullrich A, McGuire WL. Human breast cancer: correlation of relapse and survival with amplification of the HER-2/neu oncogene. Science 1987;235:177–82.
3. Lynch TJ, Bell DW, Sordella R, Gurubhagavatula S, Okimoto RA, Brannigan BW, et al. Activating mutations in the epidermal growth factor receptor underlying responsiveness of non-small-cell lung cancer to gefitinib. N Engl J Med 2004;350:2129–39.
4. Kwak EL, Bang YJ, Camidge DR, Shaw AT, Solomon B, Maki RG, et al. Anaplastic lymphoma kinase inhibition in non-small-cell lung cancer. N Engl J Med 2010;363:1693–703.
5. Flaherty KT, Puzanov I, Kim KB, Ribas A, McArthur GA, Sosman JA, et al. Inhibition of mutated, activated BRAF in metastatic melanoma. N Engl J Med 2010;363:809–19.
6. Adelstein BA, Dobbins TA, Harris CA, Marschner IC, Ward RL. A systematic review and meta-analysis of KRAS status as the determinant of response to anti-EGFR antibodies and the impact of partner chemotherapy in metastatic colorectal cancer. Eur J Cancer 2011;47:1343–54.
7. Scher HI, Morris MJ, Basch E, Heller G. End points and outcomes in castration-resistant prostate cancer: from clinical trials to clinical practice. J Clin Oncol 2011;29:3695–704.
8. Tetu B, Ro JY, Ayala AG, Johnson DE, Logothetis CJ, Ordonez NG. Small cell carcinoma of the prostate. Part I. A clinicopathologic study of 20 cases. Cancer 1987;59:1803–9.
9. Aparicio AM, Harzstark AL, Corn PG, Wen S, Araujo JC, Tu SM, et al. Platinum-based chemotherapy for variant castrate-resistant prostate cancer. Clin Cancer Res 2013;19:3621–30.
10. Aparicio A, Tzelepi V, Araujo JC, Guo CC, Liang S, Troncoso P, et al. Neuroendocrine prostate cancer xenografts with large-cell and small-cell features derived from a single patient's tumor: morphological, immunohistochemical, and gene expression profiles. Prostate 2011;71:846–56.
11. Tzelepi V, Zhang J, Lu JF, Kleb B, Wu G, Wan X, et al. Modeling a lethal prostate cancer variant with small-cell carcinoma features. Clin Cancer Res 2012;18:666–77.
12. Beltran H, Rickman DS, Park K, Chae SS, Sboner A, MacDonald TY, et al. Molecular characterization of neuroendocrine prostate cancer and identification of new drug targets. Cancer Discov 2011;1:487–95.

13. Tan HL, Sood A, Rahimi HA, Wang W, Gupta N, Hicks J, et al. Rb loss is characteristic of prostatic small cell neuroendocrine carcinoma. Clin Cancer Res 2014;20:890–903.
14. Friendly M. Corrgrams: exploratory displays for correltation matrices. Am Statistician 2002;56:316–24.
15. Cox D. Regression models and life tables (with discussion). J R Statistical Soc B 1972;34:187–220.
16. Therneau TM, Grambsch PM. Modeling survival data: extending the Cox model. New York, NY: Springer; 2000. xiii, 350 p. p.
17. SAS/STAT SIID. User's Guide, Version 9. Cary, NC: SAS Institute Inc; 2003, 2003.
18. Venables WNaR BD, editor. Modern Applied Statistics with Splus. 3rd ed. New York, NY: Springer; 1999.
19. Cerami E, Gao J, Dogrusoz U, Gross BE, Sumer SO, Aksoy BA, et al. The cBio cancer genomics portal: an open platform for exploring multidimensional cancer genomics data. Cancer Discov 2012;2:401–4.
20. Gao J, Aksoy BA, Dogrusoz U, Dresdner G, Gross B, Sumer SO, et al. Integrative analysis of complex cancer genomics and clinical profiles using the cBioPortal. Sci Signal 2013;6:pl1.
21. Robinson D, Van Allen EM, Wu YM, Schultz N, Lonigro RJ, Mosquera JM, et al. Integrative clinical genomics of advanced prostate cancer. Cell 2015;161:1215–28.
22. Lapuk AV, Wu C, Wyatt AW, McPherson A, McConeghy BJ, Brahmbhatt S, et al. From sequence to molecular pathology, and a mechanism driving the neuroendocrine phenotype in prostate cancer. J Pathol 2012;227:286–97.
23. Chatterjee SJ, George B, Goebell PJ, Alavi-Tafreshi M, Shi SR, Fung YK, et al. Hyperphosphorylation of pRb: a mechanism for RB tumour suppressor pathway inactivation in bladder cancer. J Pathol 2004;203:762–70.
24. Sharma A, Yeow WS, Ertel A, Coleman I, Clegg N, Thangavel C, et al. The retinoblastoma tumor suppressor controls androgen signaling and human prostate cancer progression. J Clin Invest 2010;120:4478–92.
25. Smith PD, Crossland S, Parker G, Osin P, Brooks L, Waller J, et al. Novel p53 mutants selected in BRCA-associated tumours which dissociate transformation suppression from other wild-type p53 functions. Oncogene 1999; 18:2451–9.
26. Li J, Yang L, Gaur S, Zhang K, Wu X, Yuan YC, et al. Mutants TP53 p.R273H and p.R273C but not p.R273G enhance cancer cell malignancy. Hum Mutat 2014;35:575–84.
27. Taylor BS, Schultz N, Hieronymus H, Gopalan A, Xiao Y, Carver BS, et al. Integrative genomic profiling of human prostate cancer. Cancer Cell 2010; 18:11–22.
28. Chen Z, Trotman LC, Shaffer D, Lin HK, Dotan ZA, Niki M, et al. Crucial role of p53-dependent cellular senescence in suppression of Pten-deficient tumorigenesis. Nature 2005;436:725–30.
29. Elgavish A, Wood PA, Pinkert CA, Eltoum IE, Cartee T, Wilbanks J, et al. Transgenic mouse with human mutant p53 expression in the prostate epithelium. Prostate 2004;61:26–34.
30. Maddison LA, Sutherland BW, Barrios RJ, Greenberg NM. Conditional deletion of Rb causes early stage prostate cancer. Cancer Res 2004;64: 6018–25.
31. Wang S, Gao J, Lei Q, Rozengurt N, Pritchard C, Jiao J, et al. Prostate-specific deletion of the murine Pten tumor suppressor gene leads to metastatic prostate cancer. Cancer Cell 2003;4:209–21.
32. Ellwood-Yen K, Graeber TG, Wongvipat J, Iruela-Arispe ML, Zhang J, Matusik R, et al. Myc-driven murine prostate cancer shares molecular features with human prostate tumors. Cancer Cell 2003;4:223–38.
33. Gingrich JR, Barrios RJ, Foster BA, Greenberg NM. Pathologic progression of autochthonous prostate cancer in the TRAMP model. Prostate Cancer Prostatic Dis 1999;2:70–5.
34. Zhou Z, Flesken-Nikitin A, Corney DC, Wang W, Goodrich DW, Roy-Burman P, et al. Synergy of p53 and Rb deficiency in a conditional mouse model for metastatic prostate cancer. Cancer Res 2006;66: 7889–98.
35. Kwabi-Addo B, Giri D, Schmidt K, Podsypanina K, Parsons R, Greenberg N, et al. Haploinsufficiency of the Pten tumor suppressor gene promotes prostate cancer progression. Proc Natl Acad Sci U S A 2001; 98:11563–8.
36. Karanika S, Karantanos T, Li L, Corn PG, Thompson TC. DNA damage response and prostate cancer: defects, regulation and therapeutic implications. Oncogene 2015;34:2815–22.
37. Nikonova AS, Astsaturov I, Serebriiskii IG, Dunbrack RL Jr, Golemis EA. Aurora A kinase (AURKA) in normal and pathological cell division. Cell Mol Life Sci 2013;70:661–87.
38. Shu SK, Liu Q, Coppola D, Cheng JQ. Phosphorylation and activation of androgen receptor by Aurora-A. J Biol Chem 2010;285:33045–53.
39. Katayama H, Sasai K, Kawai H, Yuan ZM, Bondaruk J, Suzuki F, et al. Phosphorylation by aurora kinase A induces Mdm2-mediated destabilization and inhibition of p53. Nat Genet 2004;36:55–62.
40. den Hollander J, Rimpi S, Doherty JR, Rudelius M, Buck A, Hoellein A, et al. Aurora kinases A and B are up-regulated by Myc and are essential for maintenance of the malignant state. Blood 2010;116:1498–505.
41. Ouchi M, Fujiuchi N, Sasai K, Katayama H, Minamishima YA, Ongusaha PP, et al. BRCA1 phosphorylation by Aurora-A in the regulation of G2 to M transition. J Biol Chem 2004;279:19643–8.
42. Torchia EC, Caulin C, Acin S, Terzian T, Kubick BJ, Box NF, et al. Myc, Aurora Kinase A, and mutant p53(R172H) co-operate in a mouse model of metastatic skin carcinoma. Oncogene 2012;31:2680–90.
43. Wang Y, Sun H, Wang Z, Liu M, Qi Z, Meng J, et al. Aurora-A: a potential DNA repair modulator. Tumour Biol 2014;35:2831–6.
44. Burum-Auensen E, De Angelis PM, Schjolberg AR, Kravik KL, Aure M, Clausen OP. Subcellular localization of the spindle proteins Aurora A, Mad2, and BUBR1 assessed by immunohistochemistry. J Histochem Cytochem 2007;55:477–86.
45. Nakada SY, di Sant'Agnese PA, Moynes RA, Hiipakka RA, Liao S, Cockett AT, et al. The androgen receptor status of neuroendocrine cells in human benign and malignant prostatic tissue. Cancer Res 1993;53:1967–70.
46. Epstein JI, Amin MB, Beltran H, Lotan TL, Mosquera JM, Reuter VE, et al. Proposed morphologic classification of prostate cancer with neuroendocrine differentiation. Am J Surg Pathol 2014;38:756–67.
47. Loriot Y, Massard C, Gross-Goupil M, Di Palma M, Escudier B, Bossi A, et al. Combining carboplatin and etoposide in docetaxel-pretreated patients with castration-resistant prostate cancer: a prospective study evaluating also neuroendocrine features. Ann Oncol 2009;20:703–8.
48. Shimojo M, Paquette AJ, Anderson DJ, Hersh LB. Protein kinase A regulates cholinergic gene expression in PC12 cells: REST4 silences the silencing activity of neuron-restrictive silencer factor/REST. Mol Cell Biol 1999;19: 6788–95.
49. Chaffer CL, Marjanovic ND, Lee T, Bell G, Kleer CG, Reinhardt F, et al. Poised chromatin at the ZEB1 promoter enables breast cancer cell plasticity and enhances tumorigenicity. Cell 2013;154:61–74.
50. Nathanson DA, Gini B, Mottahedeh J, Visnyei K, Koga T, Gomez G, et al. Targeted therapy resistance mediated by dynamic regulation of extrachromosomal mutant EGFR DNA. Science 2014;343:72–6.